Quantification of thermal fluctuations in stripe domain patterns

T. N. G. Meier, M. Kronseder, M. Zimmermann, and C. H. Back*
Physics Department, Universität Regensburg, Universitätsstrasse 31, 93040 Regensburg, Germany
(Received 20 April 2015; revised manuscript received 26 January 2016; published 23 February 2016)

In ultrathin ferromagnetic films with perpendicular anisotropy a spin-reorientation transition from out-of-plane to in-plane orientation of the magnetization vector may occur. The competition of exchange and dipole interaction leads to the formation of stripe domain patterns in the vicinity of the spin reorientation transition. Here we investigate fluctuations of domain patterns in ultrathin epitaxial Ni/Fe films grown on Cu(001) using the technique of threshold photoemission magnetic circular dichroism in combination with photoemission electron microscopy allowing real-time observation of the domain pattern dynamics. The key finding of our experiments is that fluctuations can easily be quantified by calculating thermodynamic susceptibilities from a series of time resolved images. We analyze the strength of fluctuations with respect to temperature and externally applied out-of-plane magnetic fields.

DOI: 10.1103/PhysRevB.93.064424

I. INTRODUCTION

Ultrathin ferromagnetic films in the stripe domain phase have attracted considerable interest in the last decades. Reasons are manifold, ranging from observing effects of the reduced dimensionality leading, e.g., to an enhanced affinity to fluctuations in the domain pattern [1–9], to special types of spiral-like reorientation transitions [10], and recently to the observation of chiral domain walls [11] connected to the emergence of the Dzyaloshinskii-Moriya interaction (DMI) in systems with broken inversion symmetry. The latter effect is linked to the appearance of nondiagonal elements in the exchange tensor creating a helical order within the domain wall and even a change of the domain wall type (Néel-to-Bloch wall transition) in ultrathin ferromagnetic layers [11]. DMI occurs due to the lack of crystal symmetry in connection with large spin-orbit interaction and it is a prerequisite for the appearance of complex spin textures [12,13].

Most of the studies concerning the research field of domain pattern and their evolution in particular in out-of-plane magnetized samples are dedicated to static properties of the domain pattern [10,14,15] or to slow dynamics of pattern transformations [16–20]. For instance, Bergeard *et al.* reported the stripe melting transition in the vicinity of the spin reorientation transition in Pt/Co/Pt films [19]. The authors could show that the melting is caused by domain wall undulations. The temporal resolution was, however, much slower than the typical time scale of individual fluctuations. Up to now, there exist only few studies which show the capability of resolving fluctuations of the domain walls on short time scales [21–23]. Recently Kronseder *et al.* investigated thermal fluctuations of topological defects with high temporal resolution in the range of milliseconds per frame [23]. Within their work fluctuation properties like dwell times or fluctuating areas were studied on individual topological defects. This article presents direct, real-time observation of fluctuations in the domain pattern of ultrathin noncentrosymmetric Ni/Fe films grown on Cu(001) with focus on thermodynamic quantities, for instance the magnetic susceptibility calculated from a large ensemble of domain states by analyzing the property of a system to sample the local energy landscape by thermal fluctuations. The susceptibility can be calculated in two ways. The first is given by the slope of $M(H)$ curves and the second is the calculation of the variance of the magnetization for an ensemble of configurations at fixed temperature and magnetic field. These two methods represent a test for the accuracy as well as the temporal resolution of the experimental setup and the calculation procedure. We find qualitative and quantitative agreement between the values of the susceptibilities extracted by using both methods.

In ultrathin ferromagnetic films the magnetization may be out-of-plane due to a positive magnetocrystalline surface or interface anisotropy and a positive magnetoelastic anisotropy due to a lattice strain in epitaxial growth. In the case of Ni/Fe/Cu(001) a positive magnetoelastic anisotropy of the nickel and iron layers exists [10,24,25]. The interface anisotropy between Ni and Fe layers is however known to be strongly negative and therefore favors in-plane orientation of the magnetization [10,24]. Hence a spin-reorientation transition can be induced if external parameters like temperature or film thickness are varied. Within this paper only the out-of-plane magnetized part of the samples is investigated. The domain pattern was imaged by using the experimental technique of threshold photoemission magnetic circular dichroism (TP-MCD) in combination with photoemission electron microscopy (PEEM). This technique provides in general a high spatial resolution of the order of 100 nm in combination with a high temporal resolution of about 1 ms. In this article, however, we only use 16.3 fps (frames per second) for our image analysis. The magnetic contrast can reach up to ≈10% for Ni/Cu(001) [26,27]. The image sequences acquired using the PEEM setup are subsequently analyzed via automated image processing.

In an out-of-plane magnetized ferromagnetic system the competition of the short-range exchange interaction and the long-range dipole interaction creates a uniform frustration and may lead to the formation of domain patterns. Early theoretical works revealed that the ground state of such a domain pattern in an ultrathin out-of-plane magnetized film is given by equally spaced parallel stripes [3,28,29]. Magnetic stripe domain patterns and spin reorientation transitions were observed in

*christian.back@ur.de

many material systems ranging from bulk systems, e.g., YIG films with thicknesses in the μm range [20,30,31], to ultrathin ferromagnetic films, e.g., Fe/Cu(001) [9,16], Fe/Ni-bilayers on Cu(001) [14,15,17,21,23,32], or Pt/Co/Pt [19,22,33]. Due to the uniform frustration in such systems even a minute amount of disorder like structural defects of the substrate leads to metastability and glassiness [34–38]. Glasslike behavior of magnetic stripe domains was already observed in garnet films [30,31] or in ultrathin Fe/Cu(001) [17]. The energy landscape of a system with competing interactions is strongly corrugated and possesses many local energy minima separated by large energy barriers [34–38]. If thermal energy is too low to overcome the barriers, the domain state may freeze in a metastable state with nearly no remaining fluctuations. Within this paper freezing of the stripe phase during cooling will be evidenced.

II. SAMPLE PREPARATION AND EXPERIMENTAL SETUP

All samples are prepared by molecular beam epitaxy (MBE) on a Cu(001) single-crystalline substrate. The base pressure of the MBE chamber is $\approx 3 \times 10^{-10}$ mbar. The substrate is cleaned by argon ion bombardment with energies of 1.2 keV for several hours prior to film deposition. After sputtering the substrate is heated to ≈800 K for 30 min to anneal the substrate. Directly before depositing the film a soft sputtering cycle at a beam voltage of 0.8 kV is carried out followed by annealing the sample at ≈800 K for less than 10 min.

Subsequently Fe and Ni films are evaporated using the method of electron-beam evaporation. A shadow mask allows the growth of wedge shaped samples. Within this paper the samples consist of a bilayer stack, where an ultrathin Fe layer is grown on Cu(001) followed by a Ni wedge with thickness ranging from 6 to 12 ML. The layer-by-layer growth is controlled by reflection high energy electron diffraction (RHEED) oscillations in combination with controlling the atomic flux.

Subsequently to the preparation of the sample it is immediately transferred into the PEEM chamber without leaving the ultrahigh vacuum environment. The base pressure in the PEEM chamber is $\approx 5 \times 10^{-11}$ mbar. The domain structure of the samples is investigated using the method of TP-MCD-PEEM, which has already been described in detail elsewhere [27]. The method is based on the creation of photoelectrons using circularly polarized light from a blue laser diode with photon energy of 3.06 eV. Information about the topography and magnetic structure of the sample is carried by photoelectrons. Since the work function of nickel is 5.15 eV [39], the photon energy of the laser diode is not sufficient to generate photoelectrons. Therefore a small amount of cesium is deposited onto the sample surface during PEEM operation to reduce the work function [21,27]. Furthermore, the PEEM chamber contains an air coil capable of applying out-of-plane magnetic fields up to 0.03 T to the sample and a liquid nitrogen cooling system offering the possibility to cool the sample to ≈170 K.

III. STATIC PROPERTIES OF THE Ni/Fe/Cu(001) SYSTEM

For the system Fe/Ni/Cu(001) the static properties of the domain pattern such as an exponential increase of the domain

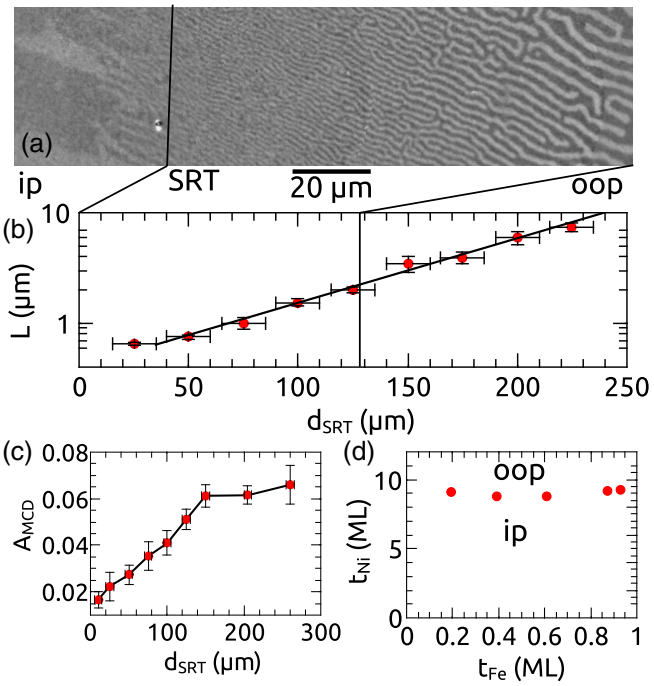

FIG. 1. Linescan of the domain pattern near the SRT of a (6–12 ML)Ni/(0–6 ML)Fe/Cu(001) double-wedge-shaped sample. (a) The highly ordered stripe domain pattern is shown near the SRT. The black line separates the in-plane phase on the left from the (canted) out-of-plane phase on the right. A minimal domain width of 0.65 μm is reached at the SRT. In (b) the domain width is plotted against the distance from the SRT d_{SRT}. The black curve in (b) shows an exponential fit to the data. The MCD asymmetry (c) decreases almost linearly when approaching the SRT indicating a continuous SRT. (d) A phase diagram of the Ni/Fe/Cu(001) system, which is determined by tracing the SRT on a double-wedge-shaped (6–12 ML)Ni/(0–3 ML)Fe/Cu(001) sample.

width with increasing distance to the SRT and a minimal domain width of ≈300 nm at the SRT are well known [14,15]. In contrast for the system Ni/Fe/Cu(001) no such measurements have been published so far. A linescan of the domain pattern in the vicinity of the SRT on a (6–12 ML)Ni/(0–6 ML)Fe/Cu(001) double-wedge sample is depicted in Fig. 1(a). A highly ordered stripe domain pattern is observed. The evolution of the domain width when approaching the SRT is plotted on a logarithmic scale in Fig. 1(b) and shows a clear exponential decrease of the domain width until a finite minimum value is reached at the SRT. This behavior is similar to the results obtained from the system Fe/Ni/Cu(001) [14,15] and predicted by the theory of Kashuba *et al.* [3,29]. A minimal domain width of 0.65 μm is measured near the SRT, which is twice as wide as for the system Fe/Ni/Cu(001) [14,15].

The analysis of the MCD asymmetry A_{MCD} allows us to characterize the direction of the magnetization vector when approaching the SRT, since $A_{\mathrm{MCD}} \propto \mathbf{M} \cdot \mathbf{h}$ with the magnetization vector $\mathbf{M}$ and the constant photon helicity $\mathbf{h}$ [26,27]. According to Millev *et al.* [40] there are three types of SRTs depending on the way the magnetization vector rotates from out-of-plane (*oop*) to in-plane (*ip*). Depending on the two- and fourfold anisotropy constants the magnetization can

show either a sharp transition from *oop* to *ip*, a continuous rotation of the magnetization via a canted state, or a hysteretic behavior at the SRT [40]. The measurement of A_{MCD} in the vicinity of the SRT plotted in Fig. 1(c) shows a continuous decrease of A_{MCD} indicating that the magnetization vector is in a canted state.

Furthermore, a phase diagram is determined for the Ni/Fe/Cu(001) system by measuring the spatial position of the SRT on a double-wedge-shaped (6–12 ML)Ni/(0–3 ML)Fe/Cu(001) sample. The resulting phase diagram is shown in Fig. 1(d). The SRT occurs around 9 ML of Ni and shows only a slight dependence on the Fe film thickness. This behavior can be attributed to the strongly negative Fe-Ni interface anisotropy term [10,24,32] and the negative Ni surface anisotropy term [24,25]. For larger Ni thicknesses the positive magnetoelastic volume anisotropy contribution of Ni leads to a SRT from the *ip* to the *oop* direction [24,25].

IV. METHOD FOR THE QUANTIFICATION OF FLUCTUATIONS

This section is dedicated to the method used for the analysis of fluctuations in magnetic domain patterns recorded by TP-MCD-PEEM. In order to get statistical averages of physical quantities movies of the domain pattern transformation each consisting of $\approx 10^3$ images are taken with a low-noise camera and a frame rate of 16.3 fps. The captured movies are subsequently analyzed using an automated image processing approach based on edge detection algorithms.

The image manipulation process starts with a polynomial fit to the raw images used for background subtraction and a referencing procedure based on pattern matching algorithms in order to compensate asynchronous motion of the camera and sample holder during acquisition. Subsequently Canny edge detection [41] is used to identify the domain walls in the images. The Canny edge detection algorithm combines high accuracy in detecting the edges with a low error rate due to a hysteresis thresholding approach. Furthermore, illumination gradients, which were not completely eliminated during background subtraction, do not affect the result since edge detection is a local operation and does not rely on global properties of the images. Subsequently an edge linking step is inserted in order to close gaps in the detected edges. Finally the individual domains are filled with either $+1$ or -1 corresponding to the sign of the z component of the magnetization. It should be noted that within the TP-MCD technique only this information can be extracted from the images, it is not possible to detect the exact direction and magnitude of the magnetization vector.

This procedure is applied to the complete sequence of images prior to the computation of magnetic and thermodynamic properties so that a set of configurations of the domain state is obtained from which statistical quantities can be calculated. The first quantity which can be determined is the geometric magnetization, which is defined as

$$m_{\mathrm{geo}} = \frac{A_\uparrow - A_\downarrow}{A_\uparrow + A_\downarrow}, \tag{1}$$

where $A_\uparrow$ and $A_\downarrow$ are the areas with magnetization up and down, respectively.

The magnetic susceptibility quantifies fluctuations of the area of the domains and is proportional to the variance of the geometric magnetization. The magnetic susceptibility is given by

$$\chi = \beta S t M_{\mathrm{S}}^2 \left(\left\langle m_{\mathrm{geo}}^2 \right\rangle - \langle m_{\mathrm{geo}} \rangle^2 \right), \tag{2}$$

where $\beta = \frac{1}{k_{\mathrm{B}} T}$, S is the surface area of the image section, $t = 1.8$ nm is the film thickness at the SRT, and M_{S} is the saturation magnetization.

The second quantity calculated from the image sequences is the exchange energy per area $\mathcal{E}_{\mathrm{ex}}$, which is described by the following equation:

$$\mathcal{E}_{\mathrm{ex}} = \frac{1}{N} \sum_{i,j} [2 - m_z(i,j) m_z(i+1,j) - m_z(i,j) m_z(i,j+1)], \tag{3}$$

where $m_z(i,j)$ is the sign of the z component of the magnetization at the pixel position (i,j) in the image and N is the total number of pixels in the image section.

Since the exchange energy is proportional to the total domain wall length, the variance of the exchange energy is a direct measure for the fluctuations of the domain walls:

$$\mathcal{C} = \left\langle \mathcal{E}_{\mathrm{ex}}^2 \right\rangle - \langle \mathcal{E}_{\mathrm{ex}} \rangle^2. \tag{4}$$

Within this paper two types of experiments concerning domain wall fluctuations are performed. In the first type the temperature of the sample is continuously decreased by cooling with a liquid nitrogen cryostat. During cooling movies of the domain pattern transformation are recorded. Upon cooling the domain width is expected to increase [3] requiring creep motion of the stripe domains in order to adopt the new equilibrium state [17,42]. The creep motion of the stripe domain endings called defects occurs in discrete steps. Between two steps of this defect motion the primary quantities (i.e., the

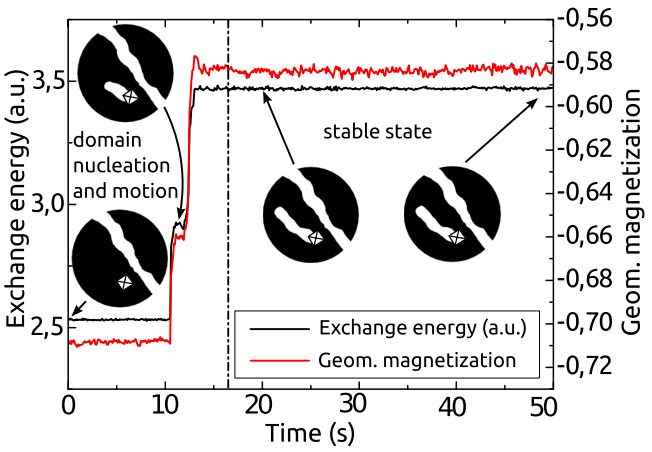

FIG. 2. Calculation of the susceptibilities. This figure shows the geometric magnetization m_{geo} and the exchange energy $\mathcal{E}_{\mathrm{ex}}$ versus time for an actual measurement, where the magnetic field is increased by a step of 0.25 Oe 2 min before recording the movie and is kept constant during the measurement. The calculation of the susceptibilities is reasonable only in periods where a stable equilibrium state is obtained (beyond the dash-dotted black line) and was done in this way throughout all calculations.

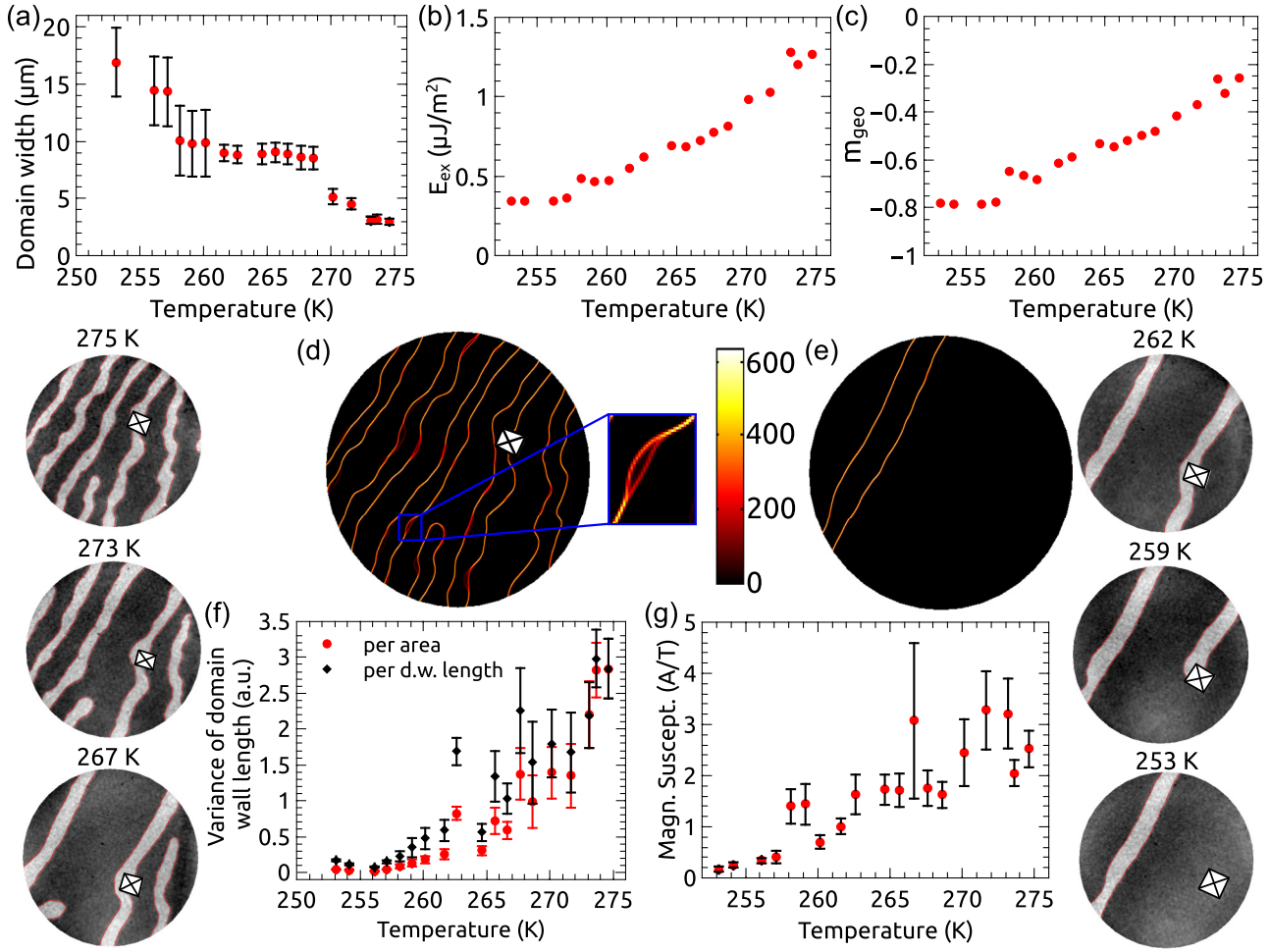

FIG. 3. Reduction of fluctuations during cooling at large domain width. The domain width (a) increases with decreasing temperature. On the left and right side of the figure representative images of the domain pattern at various temperatures are shown. The white area inside the images was not taken into account for the calculations due to a strong pinning site. The field of view of all images is 40 μm. The exchange energy per area (b) is proportional to the total domain wall length and hence decreases during cooling. The residual field of $\approx 1 \times 10^{-4}$ T in the PEEM chamber leads to a nonzero geometric magnetization, which is plotted in (c). (d) and (e) Sum images of the domain walls at 275 and 253K, respectively, reveal fluctuating areas. Red color means low occupancy of the corresponding pixel by domain walls and yellow color high occupancy. Fluctuating domain walls are therefore colored red. The inset in (d) shows the fluctuation of a domain wall between two distinct states. The variance of the total domain wall length (f) and the magnetic susceptibility (g) drastically reduce during cooling. The variance of the domain wall length is shown in two different normalizations. The red points correspond to the variance per area and the black diamonds to the variance per domain wall length.

geometric magnetization m_{geo} and the exchange energy $\mathcal{E}_{ex}$) are stable in a sense that their average values do not change over time except for small fluctuations of the domain walls, which are to be quantified within this paper. In these regions the system stays in *one* local minimum of the energy landscape and samples only a small subset of configurations [34–38]. The susceptibilities are only calculated within regions of the movies where both primary quantities are stable (see Fig. 2).

The second type of experiment is a magnetization loop, where the external magnetic field is varied at constant temperature. Since thermodynamic equilibrium is a prerequisite for the calculation of the susceptibilities, every data point within this measurement is acquired in the following way. First the magnetic field is tuned to the desired value and kept constant afterwards. Subsequently a delay time of several minutes is kept until the geometric magnetization is stable and no stripe motion or nucleation is observed any more. After reaching an equilibrium state a movie is captured and the acquired images are used for the calculation of the susceptibility (see Fig. 2). These steps are repeated for every field value.

V. QUANTIFICATION OF FLUCTUATIONS: RESULTS

A. Reduction of fluctuations during cooling

The dynamical properties of a stripe domain pattern with high degree of orientational order are investigated for a (6–12 ML)Ni/(0–3 ML)Fe/Cu(001) double-wedge-shaped sample. When cooling the system at a cooling rate of 0.4 K/min a sequence of 2000 images of the domain state is recorded at various temperatures. Each movie corresponds to a single data point in the graphs plotted in Fig. 3. The measurement starts at 275 K with an ordered stripe domain pattern (see images in Fig. 3). Upon cooling the domain

width increases indicating an increase in the perpendicular magnetic anisotropy with decreasing temperature [3]. In order to increase the domain width stripes have to withdraw from the image section. The motion of the stripes is fully discrete due to pinning. Further information about creep motion and pinning can be found elsewhere [42]. The removal of a stripe leads to an incremental increase in the domain width which can also be seen in the average domain width in the image section plotted in Fig. 3(a). Due to the increasing domain width the total domain wall length decreases as well as the exchange energy as shown in Fig. 3(b). Note that the domain walls become more straight with decreasing temperature. This fact indicates that the domain wall dynamics is governed by the elastic energies [3] and not by pinning potentials. In the case of strong pinning the domain walls would get rougher with decreasing temperature. A detailed description of the mechanisms of pattern transformations will be published elsewhere [43]. At 250 K the last stripe withdraws from the image section and a uniform magnetization state is reached.

A residual field of the order of 1×10^{-4} T in the PEEM chamber magnetizes the sample so that a nonzero geometric magnetization is obtained, as can be seen in Fig. 3(c). The increase of the geometric magnetization during cooling can be explained by a decrease of the critical field, at which all domains are annihilated. According to Kashuba *et al.* the critical field is proportional to the inverse domain width [3,29].

Due to thermal activation domain walls fluctuate. The local dependence of fluctuations reveals thereby the distribution of pinning sites stronger than the average thermal energy, which can be visualized by summing up the domain walls of all images of a movie. The result is plotted using a colormap, where red indicates low occupancy of a certain pixel by a domain wall and yellow high occupancy. Fluctuating domain walls are therefore visualized as red lines in such an image. Sum images of the domain walls are plotted for the temperatures 275 and 253 K in Figs. 3(d) and 3(e), respectively. By comparison of the two images the reduction of fluctuations during cooling becomes apparent. This qualitative observation can be quantified using the thermodynamic susceptibilities. Figures 3(f) and 3(g) show the variance of the total domain wall length and the magnetic susceptibility, respectively. Both quantities decrease strongly by more than one order of magnitude. Note that the susceptibilities almost reach a value around zero at the lowest temperature indicating that the systematic errors caused by the image processing are very low. The reduction of the variance of the total domain wall length per area [red points in Fig. 3(f)] is caused by two effects. The first is the reduction of the domain wall length and the second is the reduction of the local fluctuations per domain wall length. In order to disentangle these contributions the variance per domain wall length is calculated [black diamonds in Fig. 3(f)]. Since the variance per area decreases by a factor of 63 and the total domain wall length only by a factor of 3.7 during cooling, the reduction of the variance per area is mostly due to the reduction of the local fluctuations per domain wall length and the decrease of the total domain wall length is only a smaller effect.

In contrast to the previous measurement, which has been carried out far away from the SRT at a large initial domain width of $\approx 4\ \mu$m, a second cooling experiment is performed

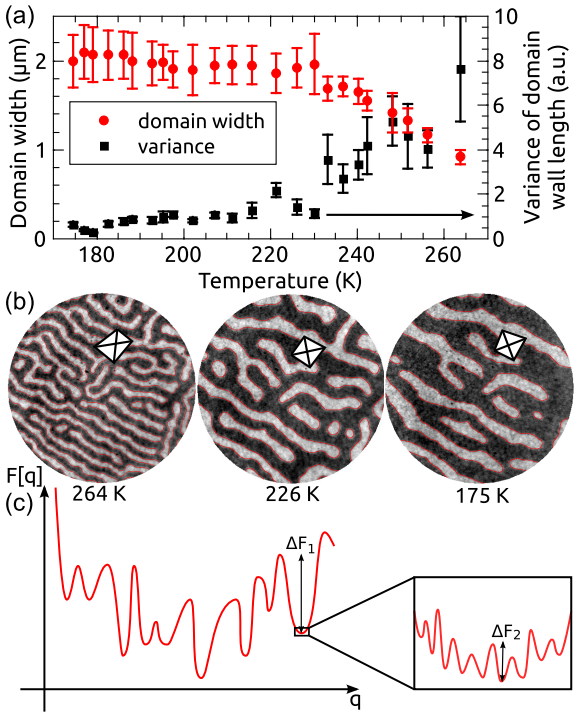

FIG. 4. Cooling in the vicinity of the SRT. (a) The evolution of the domain width (red dots) as well as the variance of the total domain wall length (black squares) versus temperature. Images of the domain pattern at various temperatures are depicted in (b). During cooling the domain width increases at first accompanied by a strong reduction of the fluctuations of the domain walls. Below 230 K the domain pattern becomes stationary. This is explainable in terms of a strongly corrugated energy landscape, which is exemplary visualized in (c), where the free energy is plotted versus configuration coordinates q of the system. If thermal energy is much lower than ΔF_1 the system gets trapped in the local minimum of the energy landscape and may stay there a long time. The system is nonergodic and samples only a smaller subset of configurations inside the local minimum if thermal energy is on the order of or larger than ΔF_2.

on the same sample but closer to the SRT with an initial domain width of 0.9 μm. Figure 4(a) shows the evolution of the domain width during cooling with a cooling rate of 1.9 K/min. With decreasing temperature the domain width increases at first as in the experiment before. Below 230 K no significant change in the domain width can be recognized. The images of the domains in Fig. 4(b) clearly show that the domain pattern becomes stationary for temperatures below 230 K. Upon cooling fluctuations of the domain pattern quantified by the variance of the domain wall length plotted as black squares in Fig. 4(a) are strongly reduced in the beginning, comparable to the first measurement in Fig. 3(f). In the frozen state below 230 K a small, but measurable amount of fluctuations remains. Note that in the previous experiment the variance of the domain wall length obtains much smaller values at the same temperature than here, Figs. 3 (f) and 4(a).

The freezing of the domain pattern can be explained in terms of a strongly corrugated energy landscape with large barriers between sets of states [34–38]. If thermal energy is reduced by cooling the sample, the relaxation time increases exponentially by a Vogel-Fulcher law [35–38] and the barriers

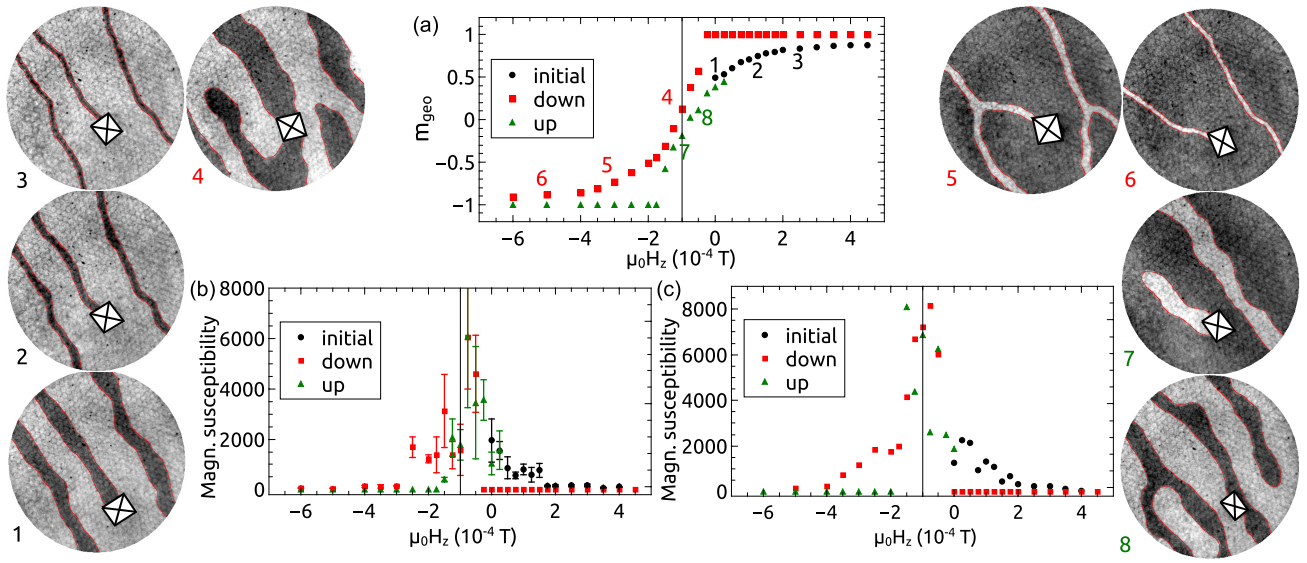

FIG. 5. Application of out-of-plane magnetic fields to a (6–12 ML)Ni/(0–3 ML)Fe/Cu(001) sample. The measurement is carried out at room temperature at a Ni thickness of ≈9 ML and a Fe thickness of ≈1 ML. (a) Magnetization loop. Starting from zero applied field the initial curve (black dots) has been recorded. The subsequent down sweep of the magnetic field is plotted as red squares and the final sweep back to zero applied field as green triangles. The images on the left and right side of the figure show the domain pattern at certain values of the applied magnetic field. Note that the loop is shifted by $\approx 1 \times 10^{-4}$ T indicating the presence of a residual field inside the PEEM chamber. The black line in the plots is a guide to the eye for zero field. In (b) and (c) the magnetic susceptibilities are plotted versus the applied magnetic field. In (b) the susceptibility is calculated from fluctuations in the domain pattern and in (c) from the derivative of the magnetization loop shown in (a) with respect to the magnetic field, which is approximated by the difference quotient. Both graphs are in good agreement and show that fluctuations in the domain pattern are maximal around zero field and are drastically reduced in high magnetic fields.

in the energy landscape might be too high to be overcome in an experimentally accessible time scale. The system gets trapped in a metastable state inside one of the local energy minima of the energy landscape. In this case the system is nonergodic, but still samples a small subset of reachable states inside this local energy minimum so that some fluctuations of the domain pattern remain, see Fig. 4(c).

B. Application of magnetic fields

In the following the transformation of domain patterns while sweeping the externally applied magnetic field is investigated for the system (6–12 ML)Ni/(0–3 ML)Fe/Cu(001). Figure 5 shows the geometric magnetization and representative images of the domain pattern for various values of the applied magnetic field. Note that after applying a certain field value and before a sequence of images is taken, we wait for 2 min in order to reach an equilibrium state of the sample.

The behavior of an out-of-plane magnetized 2D ferromagnetic film in a magnetic field has been predicted by Kashuba *et al.* [3,29] in the following two senses. First, with increasing magnetic field the average domain width, i.e., the average of minority and majority domain width, increases and finally diverges at the so called critical magnetic field above which the sample is in a uniform state [3]. Second, the minority domain width decreases with increasing magnetic field but converges against a nonzero minimum value at the critical field [3]. This is in qualitative agreement with the experiment. In images 3 and 6 in Fig. 5 the minority spin domains have reached their smallest size and do not shrink further while increasing the magnetic field.

The transformation of the domain pattern by applying a magnetic field can be divided into two regimes. In the range of low field values the transformation is governed by a reduction of the width of minority domains and no stripe annihilation or defect motion can be observed (compare images 1–3 in Fig. 5). This leads to a paramagneticlike response of the domain pattern at low magnetic fields evidenced by the linear evolution of the geometric magnetization with respect to the applied magnetic field in Fig. 5(a) [44]. In the second regime for higher fields the Zeeman energy is large enough to overcome pinning sites and stepwise annihilation of the stripes further increases the geometric magnetization (see images 5 and 6 in Fig. 5) until the sample is in a uniform state. If the magnetic field is subsequently reduced below a certain field value, stripe domains nucleate. Note that nucleation of domains preferentially takes place at impurities of the sample (compare with image 7 in Fig. 5) [17].

Next the dependence of fluctuations on the applied magnetic field is investigated by calculating the magnetic susceptibility. The magnetic susceptibility can, on the one hand, be extracted from fluctuations of the domain pattern quantified by the variance of the geometric magnetization [Eq. (2)]. On the other hand, the magnetic susceptibility is also given by the derivative of the geometric magnetization with respect to the externally applied magnetic field:

$$\chi = M_S \frac{\partial m_{geo}}{\partial H_z}. \tag{5}$$

The derivative of the magnetization is approximated by the difference quotient of the geometric magnetization plotted in Fig. 5(a). Note that these two calculations of the magnetic

susceptibility originate from completely different approaches. The results for both approaches are plotted in Figs. 5(b) and 5(c). With increasing magnetic field the magnetic susceptibility decreases. Due to the small width of the minority domains at high fields their compression constant within the model of elastic domain wall theory proposed in [3] is very large so that compressive distortions of the small stripes are energetically unfavorable and the domain walls strongly repel each other [33]. This strong repulsion of neighboring domain walls leads to the suppression of fluctuations at high magnetic fields. Note that there is a good quantitative as well as qualitative agreement between both methods of calculation for the magnetic susceptibilities.

VI. CONCLUSION

In this paper fluctuations of magnetic stripe domains in the bilayer system Ni/Fe/Cu(001) are analyzed by real-time observation of the domain pattern using the TP-MCD-PEEM technique. The magnetic susceptibility and variance of the total domain wall length was investigated with respect to the sample temperature as well as out-of-plane externally applied magnetic fields by quantitative examination of fluctuations in the domain pattern. Cooling the sample at large domain width leads to a strong reduction of fluctuations, which was qualitatively as well as quantitatively demonstrated within this paper, until a uniform state of the magnetization is reached. If the cooling experiment is in contrast performed in the vicinity of the SRT, the domain pattern freezes into a metastable, maybe glassy state with a low, but measurable amount of residual domain fluctuations. This behavior is a clear evidence for a strongly corrugated energy landscape with high barriers, which is typical for a glassy system [34,35]. The application of out-of-plane magnetic fields forces the antiparallely magnetized domains to shrink accompanied by a reduction of fluctuations of the domains due to the enhanced compression constant of the minority stripe domains. In addition, two individual approaches to calculate the magnetic susceptibilities (via fluctuations and derivative of the geometric magnetization) have led to a qualitative as well as quantitative agreement.

[1] H. E. Stanley, *Phase Transitions and Critical Phenomena*, Vol. 1 (Clarendon, Oxford, 1971).

[2] A. Z. Patashinskii, and V. L. Pokrovskii, *Fluctuation Theory of Phase Transitions* (Elsevier, Amsterdam, 1979).

[3] A. B. Kashuba and V. L. Pokrovsky, Phys. Rev. B **48**, 10335 (1993).

[4] A. Abanov, V. Kalatsky, V. L. Pokrovsky, and W. M. Saslow, Phys. Rev. B **51**, 1023 (1995).

[5] K. De'Bell, A. B. MacIsaac, and J. P. Whitehead, Rev. Mod. Phys. **72**, 225 (2000).

[6] A. D. Stoycheva and S. J. Singer, Phys. Rev. Lett. **84**, 4657 (2000).

[7] L. Nicolao and D. A. Stariolo, Phys. Rev. B **76**, 054453 (2007).

[8] M. Carubelli, O. V. Billoni, S. A. Pighin, S. A. Cannas, D. A. Stariolo, and F. A. Tamarit, Phys. Rev. B **77**, 134417 (2008).

[9] O. Portmann, A. Gölzer, N. Saratz, O. V. Billoni, D. Pescia, and A. Vindigni, Phys. Rev. B **82**, 184409 (2010).

[10] R. Ramchal, A. K. Schmid, M. Farle, and H. Poppa, Phys. Rev. B **69**, 214401 (2004).

[11] G. Chen, J. Zhu, A. Quesada, J. Li, A. T. N'Diaye, Y. Huo, T. P. Ma, Y. Chen, H. Y. Kwon, C. Won, Z. Q. Qiu, A. K. Schmid, and Y. Z. Wu, Phys. Rev. Lett. **110**, 177204 (2013).

[12] N. Nagaosa and Y. Tokura, Nat. Nanotechnol. **8**, 899 (2013).

[13] M. Mochizuki, X. Z. Yu, S. Seki, N. Kanazawa, W. Koshibae, J. Zang, M. Mostovoy, Y. Tokura, and N. Nagaosa, Nat. Mater. **13**, 241 (2014).

[14] C. Won, Y. Z. Wu, J. Choi, W. Kim, A. Scholl, A. Doran, T. Owens, J. Wu, X. F. Jin, and Z. Q. Qiu, Phys. Rev. B **71**, 224429 (2005).

[15] Y. Z. Wu, C. Won, A. Scholl, A. Doran, H. W. Zhao, X. F. Jin, and Z. Q. Qiu, Phys. Rev. Lett. **93**, 117205 (2004).

[16] O. Portmann, A. Vaterlaus, and D. Pescia, Nature (London) **422**, 701 (2003).

[17] N. Saratz, T. Michlmayr, O. Portmann, U. Ramsperger, and A. Vaterlaus, J. Phys. D **40**, 1268 (2007).

[18] J. Wu, J. Choi, C. Won, Y. Z. Wu, A. Scholl, A. Doran, C. Hwang, and Z. Q. Qiu, Phys. Rev. B **79**, 014429 (2009).

[19] N. Bergeard, J. P. Jamet, A. Mougin, J. Ferré, J. Gierak, E. Bourhis, and R. Stamps, Phys. Rev. B **86**, 094431 (2012).

[20] W. Jiang, Y. Fan, P. Upadhyaya, M. Lang, M. Wang, L.-T. Chang, K. L. Wong, J. Tang, M. Lewis, J. Zhao, L. He, X. Kou, C. Zeng, X. Z. Zhou, R. N. Schwartz, and K. L. Wang, Phys. Rev. B **87**, 014427 (2013).

[21] M. Kronseder, M. Buchner, H. G. Bauer, and C. H. Back, Nat. Commun. **4**, 2054 (2013).

[22] A. L. Balk, M. D. Stiles, and J. Unguris, Phys. Rev. B **90**, 184404 (2014).

[23] M. Kronseder, T. N. G. Meier, M. Zimmermann, M. Buchner, M. Vogel, and C. H. Back, Nat. Commun. **6**, 7832 (2015).

[24] H. Abe, K. Amemiya, D. Matsumura, S. Kitagawa, H. Watanabe, T. Yokoyama, and T. Ohta, J. Magn. Magn. Mater. **302**, 86 (2006).

[25] W. L. O'Brien, T. Droubay, and B. P. Tonner, Phys. Rev. B **54**, 9297 (1996).

[26] T. Nakagawa and T. Yokoyama, Phys. Rev. Lett. **96**, 237402 (2006).

[27] M. Kronseder, J. Minár, J. Braun, S. Günther, G. Woltersdorf, H. Ebert, and C. H. Back, Phys. Rev. B **83**, 132404 (2011).

[28] Y. Yafet and E. M. Gyorgy, Phys. Rev. B **38**, 9145 (1988).

[29] A. Kashuba and V. L. Pokrovsky, Phys. Rev. Lett. **70**, 3155 (1993).

[30] M. Seul and R. Wolfe, Phys. Rev. A **46**, 7534 (1992).

[31] B. Reimann, R. Richter, and I. Rehberg, Phys. Rev. E **65**, 031504 (2002).

[32] H. W. Zhao, C. Won, Y. Z. Wu, A. Scholl, A. Doran, and Z. Q. Qiu, Phys. Rev. B **70**, 024423 (2004).

[33] M. Bauer, A. Mougin, J. P. Jamet, V. Repain, J. Ferré, R. L. Stamps, H. Bernas, and C. Chappert, Phys. Rev. Lett. **94**, 207211 (2005).

[34] J. Schmalian and P. G. Wolynes, Phys. Rev. Lett. **85**, 836 (2000).

[35] M. Dzero, J. Schmalian, and P. G. Wolynes, arXiv:1011.2261,

Structural Glasses and Supercooled Liquids: Theory, Experiment, and Applications (John Wiley and Sons, New York, 2012).
[36] F. H. Stillinger, Science **267**, 1935 (1995).
[37] P. G. Debenedetti and F. H. Stillinger, Nature (London) **410**, 259 (2001).
[38] H. Westfahl, J. Schmalian, and P. G. Wolynes, Phys. Rev. B **64**, 174203 (2001).
[39] D. E. Eastman, Phys. Rev. B **2**, 1 (1970).
[40] Y. Millev and J. Kirschner, Phys. Rev. B **54**, 4137 (1996).
[41] J. Canny, IEEE Trans. Pattern Anal. Machine Intell. **PAMI-8**, 679 (1986).
[42] P. Chauve, T. Giamarchi, and P. Le Doussal, Phys. Rev. B **62**, 6241 (2000).
[43] M. Zimmermann, T. N. G. Meier, M. Kronseder, and C. H. Back (unpublished).
[44] D. Venus and M. Dunlavy, J. Magn. Magn. Mater. **260**, 195 (2003).